RSC Advances

PAPER

Cite this: *RSC Adv.*, 2021, **11**, 13545

Magnetic polymer bowl for enhanced catalytic activity and recyclability†

Sang Gi Hong,[a] Eunmi Im,‡[b] Da In Kim,[a] Eun Jin Jeong,[b] Jongbok Kim,[cd] Geon Dae Moon*[b] and Dong Choon Hyun*[a]

Received 19th January 2021
Accepted 7th April 2021

DOI: 10.1039/d1ra00453k

rsc.li/rsc-advances

This work introduces the fabrication of a magnetic polymer bowl for enhanced catalytic activity and recyclability, which involves the synthesis of silica-coated Fe_3O_4 magnetic clusters, seeded dispersion polymerization using the magnetic clusters, and transformation into a bowl-like structure *via* a phase separation route. The additional treatment with tannic acid (TA) on the bowls allows the *in situ* formation of silver nanoparticles (AgNPs) on their surfaces. The openness and larger surface area of the bowls, as compared with those of other structured particles, such as spheres and flowers, enable a considerably higher immobilization of AgNPs, thus leading to an excellent catalytic reduction for 4-nitrophenol (4-NP), methylene blue (MB), and rhodamine B. Furthermore, the strong magnetic response originating from the magnetic clusters inside the bowls endows a good magnetic recovery and an excellent reusability for the repeated reduction of the organic dyes without loss of catalytic activity.

Introduction

With the rapid growth of industrialization and population, modern society has suffered from environmental pollution.[1] Especially, inflow of effluent containing organic dyes into water resources causes serious environmental problems because the strong color of dyes can block oxygen and sunlight from penetrating the water.[2] Furthermore, toxicity of organic dyes can threaten human health.[3] As a representative organic dye distributed from agricultural and industrial areas, 4-nitrophenol (4-NP), which is responsible for methemoglobinemia, can cause cyanosis, confusion, and unconsciousness as well as damage to the liver and kidneys.[4,5] Rhodamine B and methylene blue (MB) exhibit toxicity and carcinogenicity, which can cause numerous severe diseases.[6,7] Thus, the development of an efficient approach to remove harmful organic dyes from contaminated water is essentially needed.

Among several techniques developed for the removal of organic dyes, chemical approaches using nanomaterial catalysts, which can convert organic dyes into non-/less toxic or useful products through change in their molecular structures, have recently gained considerable attention owing to its high efficiency, low cost, and simple setups.[8,9] For example, 4-NP can be reduced to 4-aminophenol (4-AP) in the presence of catalysts and reductants, which is a useful compound in pharmaceutical industry.[10] Similarly, rhodamine B and MB can be reduced to colorless compounds (leuco rhodamine B and leuco MB) with the use of proper catalysts in the presence of $NaBH_4$.[11,12] When catalytic activity and chemical/physical stability are concerned, noble metal nanoparticles (NPs), including platinum (Pt), silver (Ag), and gold (Au) have been considered as the optimal catalysts.[2,13,14] However, the poor colloidal stability, originating from their high surface area, and difficulty in separation cause the decrease of active sites and catalytic performance for the reduction of organic dyes.[15] In addressing this issue, the use of various supports to deposit noble metal NPs on their surfaces has been reported.[16] Among them, polystyrene (PS) particles have shown numerous advantages as a catalytic support material, such as their simple and large scalable synthesis, monodispersity and controllability in size and shape, good dispersion in various media, and easy surface modification.[17–20] Because most of previously reported studies have used, however, solid PS particles with a relatively low surface area,[20–26] it is difficult to increase the loading amount of noble metal NPs. Alternatively, numerous studies have reported the fabrication of PS particles with hollow structures to provide large surface areas.[27] However, the closed shells in most of the hollow particles allow the deposition of noble metal NPs only on the outer surfaces, not exhibiting a higher deposition of noble metal NPs compared with solid PS particles. Furthermore, their limited recovery from

[a]*Department of Polymer Science and Engineering, School of Applied Chemical Engineering, Polymeric Nano-materials Laboratory, Kyungpook National University, Daegu 41566, South Korea. E-mail: dong.hyun@knu.ac.kr*

[b]*Dongnam Division, Korea Institute of Industrial Technology, Busan 46938, Korea. E-mail: gmoon@kitech.re.kr*

[c]*Department of Materials Science and Engineering, Kumoh National Institute of Technology, Gumi, Gyeongbuk 39177, Korea*

[d]*Department of Energy Engineering Convergence, Kumoh National Institute of Technology, Gumi 39177, Korea*

† Electronic supplementary information (ESI) available. See DOI: 10.1039/d1ra00453k

‡ These authors contributed equally to the preparation of this paper.

reaction system by centrifugation or filtration causes a poor reusability during cycles of catalytic process, consequently hindering their practical applications to the treatment of toxic organic dyes.

In this study, we demonstrate the fabrication of a magnetic polymer bowl for the enhanced catalytic activity and recyclability. The magnetic polymer bowl is prepared through synthesis of silica-coated Fe_3O_4 magnetic clusters, their surface treatment with vinyl group, and seeded dispersion polymerization under the use of the magnetic clusters, followed by phase separation for the transformation into bowl-like structure (Scheme 1). The additional treatment with tannic acid (TA) on the bowls allows the *in situ* formation of AgNPs on their surfaces. The openness and larger surface area of the bowls, as compared with those of other structured-particles such as spheres and flowers, enable a considerably higher immobilization of AgNPs, leading to an excellent catalytic reduction for 4-NP, rhodamine B, and MB. Furthermore, the strong magnetic response arising from the magnetic clusters inside the bowls endows a good magnetic recovery and an excellent reusability, achieving twenty consecutive reduction of the dye molecules with no loss in catalytic activity.

Experimental

Materials

Poly(4-styrenesulfonic acid-*co*-maleic acid, SS : MA = 3 : 1) sodium salt (PSSMA, M_W = 20 000), styrene (St), tetraethyl orthosilicate (TEOS), silver nitrate ($AgNO_3$), decane, TA, 4-NP, rhodamine B, MB, anhydrous sodium acetate (NaOAc), sodium 4-vinylbenzenesulfonate (NaSS), ethylene glycol (EG), ammonium hydroxide (NH_4OH) solution, 2-ethylhexyl methacrylate (EHMA), 3-(trimethoxysilyl)propyl methacrylate (MPS), ferric chloride ($FeCl_3$), isoamyl alcohol, ferric chloride hexahydrate ($FeCl_3 \cdot 6H_2O$), and azobisisobutyronitrile (AIBN) were obtained from Sigma-Aldrich. All chemicals were used as received without further purification. Deionized (DI) water with a resistivity of 18.2 MΩ cm, purified by a water ultra-purification system (ROMAX, Human Science), was utilized for silica coating, preparation of organic dye solutions, and dispersion of particles.

Synthesis of Fe_3O_4 magnetic clusters and their coating with silica

Using the modified solvothermal method, Fe_3O_4 magnetic clusters were synthesized, as reported previously.[28] Briefly, a PSSMA solution was first prepared by dissolving 0.5 g of the polymer into 20 mL of EG under vigorous stirring, followed by additionally introducing 0.54 g of $FeCl_3 \cdot 6H_2O$ and 1.5 g of NaOAc. After sealing the mixture solution in a Teflon-lined stainless-steel autoclave, the system was heated to 200 °C for 10 h. The sample was then cooled to room temperature, followed by centrifugation (4500 rpm, 15 min), washing with DI water, and vacuum-drying for 24 h. For coating the Fe_3O_4 magnetic clusters with silica, the dried clusters were mixed with a co-solvent consisting of 100 mL of ethanol and 15 mL of DI water, followed by injecting 5 mL of NH_4OH solution and 1 mL of TEOS. After 3 h, the resultant clusters, separated by a magnet, were consecutively washed with ethanol and DI water.

Fabrication of magnetic polymer spheres and flowers

After the silica-coated magnetic clusters (0.5 g) were mixed with 100 mL of ethanol, MPS was injected. The mixture solution was mechanically agitated at room temperature to induce the formation of vinyl groups on the surfaces of the silica-coated magnetic clusters. Subsequently, the mixture solution was washed with ethanol and DI water. The MPS-treated clusters (0.12 g) were introduced into a co-solvent with 70 mL of ethanol and 30 mL of DI water, together with 0.06 g of AIBN, 0.03 g of NaSS, and 3 mL of St. After mechanical agitation for 30 min, the mixture solution was heated to 70 °C for 6 h under a nitrogen (N_2) atmosphere. Then, the resultant particles were separated with a magnet, washed with ethanol and DI water, and dried in vacuum.

Transformation of magnetic polymer sphere into magnetic polymer bowls

First, 0.025 g of the magnetic polymer spheres was put into a glass vial with 10 mL of methanol and 2 mL of DI water, followed by successively adding 0.006 g of AIBN, 0.642 mL of decane, and 0.124 mL of EHMA. Under N_2 atmosphere and

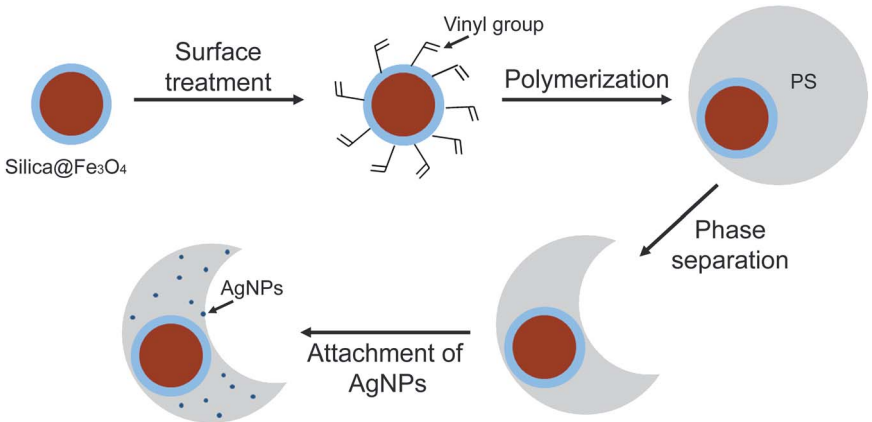

Scheme 1 Schematic illustration of the procedure for fabricating magnetic polymer bowl with highly immobilized AgNPs.

mechanical agitation, the mixture solution was heated to 70 °C for 2 h. After the resultant particles were separated with a magnet, the decane, unreacted reagents, and polymerized EHMA were removed from the particles using ethanol and isoamyl alcohol.

In situ formation of AgNPs

An aqueous $FeCl_3$ solution (200 μL, 10 mg mL^{-1}) was injected into 20 mL of an aqueous dispersion of magnetic polymer particles (1 mg mL^{-1}) under mechanical agitation. After 1 min, the magnetic polymer particles were separated by a magnet, followed by washing with DI water and dispersing again in 20 mL of DI water. Subsequently, 200 μL of an aqueous TA solution (40 mg mL^{-1}) was injected into the dispersion under mechanical agitation, followed by separating with a magnet and washing with DI water. The resultant particles were treated again with $FeCl_3$ and TA in the same way as described previously and then dispersed again in 10 mL of DI water. To form AgNPs on the magnetic polymer particles, 30 μL of $Ag(NH_3)_2OH$ solution, which was prepared using an aqueous $AgNO_3$ solution (10 mL, 0.1 M) and an NH_4OH solution (200 μL), was injected into the dispersion of the magnetic polymer particles. After mild agitation for 1 h, separation with a magnet and washing with DI water were consecutively carried out.

Catalytic test

To examine the catalytic performance of magnetic polymer particles with immobilized AgNPs on their surfaces, an aqueous $NaBH_4$ solution (1 mL, 40 mM) was mixed with an aqueous 4-NP solution (1 mL, 0.4 mM), to which 3 mL of a dispersion of AgNP-immobilized, magnetic polymer particle (2.1×10^7 particles mL^{-1}) was additionally injected. For rhodamine B, a dispersion of AgNP-immobilized, magnetic polymer particles (3 mL, 2.1×10^7 particles mL^{-1}) was introduced into 2 mL of an aqueous solution with rhodamine B solution (0.05 mM) and $NaBH_4$ (5 mM). The reduction of MB was tested by introducing a dispersion of AgNP-immobilized, magnetic polymer particles (3 mL, 2.1×10^7 particles mL^{-1}) into 2 mL of a mixture solution pre-containing 10 mM of $NaBH_4$ and 0.1 mM of MB. The reduction reactions of the organic dye molecules were monitored *via* UV-vis spectrometry (T60, PG Instruments). Moreover, the conversion extents were determined from the absorbance peak intensities (I_{400}, I_{554}, and I_{664}) at 400, 554, and 664 nm for 4-NP, rhodamine B, and MB, respectively. To test the reusability of the AgNP-immobilized, magnetic polymer particles for catalytic reduction, they were separated from the reaction solution with a magnet after each cycle of the reduction and washed with DI water. Then, the resultant particles were utilized for the next cycle of reduction.

Characterization

Scanning electron microscopy (SEM, SU-8220, Hitachi) was used to study the surface structure of the magnetic polymer particles. The inside structures of the magnetic polymer particles and the immobilization of AgNPs on their surfaces were examined using a transmission electron microscope (TEM, HT-7700, Hitachi) equipped with an energy-dispersive X-ray spectrometer (EDS). The high resolution TEM (HRTEM) image of the magnetic cluster was taken using a Titan G2 ChemiSTEM operated at 200 kV (FEI Company). The surface charge properties of the magnetic polymer particles treated with $FeCl_3$ and TA were measured by a zeta-potential analyzer (Nano ZS zetasizer, Malvern Instruments). X-ray diffraction (XRD) pattern of Fe_3O_4 magnetic clusters was obtained with the use of an X-ray diffractometer (D/MAX-2500, Rigaku) with a Cu Kα radiation source. The elements present in the magnetic polymer particles with attached AgNPs were investigated using an X-ray photoelectron spectrometer (XPS, Quantera SXM, ULVAC-PHI). The number of AgNPs attached on a magnetic polymer particle was determined by employing inductively coupled plasma mass spectrometry (ICP-MS, NexION 2000, PerkinElmer).

Results and discussion

To enable repeated use of magnetic polymer particles, they should be easily collected in response to moderate magnetic field. Magnetic nanocrystals with dimensions on the order of 10 nm are known to exhibit low magnetization per particle,[29] thus essentially requiring the use of an extremely strong field. Growth of the nanocrystal in size exhibits an increase in saturation magnetization, but at the expense of the superparamagnetism.[29] Magnetic clusters with assembly of multiple magnetic nanocrystals have many merits, including high magnetic susceptibility, superparamagnetism, and low coercive force.[30,31] With these regards, we chose to use Fe_3O_4 magnetic clusters as seeds to synthesize magnetic polymer particles. A TEM image of the magnetic clusters synthesized by employing the modified solvothermal method is shown in Fig. 1A. The formation of particles with nearly spherical shape was observed, and their mean diameter, which was obtained using the TEM image, was 254 ± 24 nm. Fig. 1B shows an HRTEM image for the white-boxed region in Fig. 1A. Many nanocrystals with a diameter of 7–9 nm were assembled together to form the magnetic clusters. The corresponding electron diffraction (ED) pattern recorded on the single cluster contained 220, 311, 400, 511, and 440 diffractions, as shown in the inset. A similar result was also observed through XRD measurement. As shown in Fig. 1C, six characteristic peaks appeared at $2\theta = 30.2°$, 35.5°, 43.1°, 53.4°, 57.1°, and 62.8°, which corresponded to (220), (311), (400), (422), (511), and (440) of Fe_3O_4, respectively.[14] These results indicate that the small nanocrystals were Fe_3O_4. Using the Scherrer's equation and the strongest diffraction peaks indexed to (311), we could estimate the average crystallite size and the calculated value was 7.5 nm, which was in line with to the result reported previously.[28] The saturation magnetization of the magnetic clusters was measured with a vibrating sample magnetometer (VSM), which was determined to be 75.8 emu g^{-1} at room temperature (Fig. S1, ESI†). This high magnetization moved all the clusters in their aqueous dispersion toward an external magnet in 2 min (Fig. 1D), indicating that they were magnetically responsive.

The surfaces of the magnetic clusters were silica-coated for enhancing their chemical stability and acid resistance, as well as for conducting further chemical reactions to make magnetic

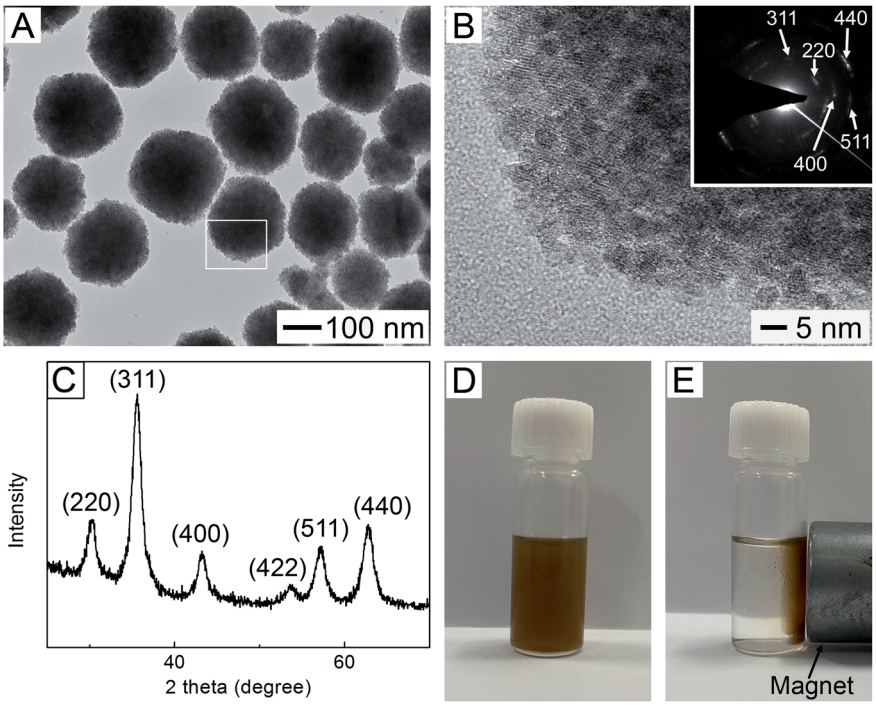

Fig. 1 (A) TEM image of the Fe_3O_4 magnetic clusters synthesized using the modified solvothermal method. (B) HRTEM image of the white-boxed region in (A). The inset shows an ED pattern of the single magnetic cluster. (C) XRD pattern of the as-synthesized Fe_3O_4 magnetic clusters. (D and E) Photographs of the Fe_3O_4 magnetic clusters dispersed in DI water: (D) without and (E) with application of a magnet.

polymer particles. In this study, the Stöber method, which has been mainly employed for silica coating,[32] was used. Fig. 2A shows a TEM image of the magnetic clusters obtained after the treatment using the Stöber method, demonstrating the formation of spherical particles that consist of single magnetic cores and silica shells with uniform thickness. The silica-coated magnetic clusters had a mean diameter of 401 ± 21 nm. Using this result and the diameter of the magnetic clusters in Fig. 1A, the coating layer thickness was calculated to be about 73 nm, which was also confirmed in the inset image. The XRD pattern of the silica-coated sample was the same as that of the magnetic clusters in Fig. 1C (Fig. S2A, ESI†), suggesting that the coating did not affect the crystalline structure of the magnetic cluster cores. Consequently, the silica-coated particles still retained a strong magnetic response driven by the magnetic cores (Fig. S2B and C†).

These silica-coated particles were employed as seeds for preparing magnetic polymer particles. When we carried out the polymerization using the particles in Fig. 2A as seeds, the PS particles separated from the magnetic seeds were made (Fig. S3, ESI†), indicating no interaction between both of the two components. To improve the interaction, the silica-coated particles were modified with MPS to induce the formation of vinyl groups on their surfaces. We controlled the grafting density of MPS by varying its treatment conditions, such as the volume of MPS and treatment time, followed by determining the density value (Q_{MPS}, μmol m^{-2}) using UV-vis spectrometry (see ESI†). When the silica-coated magnetic clusters were treated with 1 mL of MPS for 24 h, the calculated Q_{MPS} was 1 μmol m^{-2}. The incubation with 2 mL of MPS for 5 days increased the value of Q_{MPS} to 4.5 μmol m^{-2}. Fig. 2B shows a TEM image of the particles made by the polymerization at 70 °C for 6 h under the use of the MPS-treated seeds with Q_{MPS} of 1 μmol m^{-2}, which demonstrates the formation of flower-like particles, consisting of PS nodules attached to one seed. This result was because the MPS treatment promoted favorable interactions between the seed and polymer species, leading to a covalent grafting of PS chains on the surfaces of the seeds.[33] As shown in Fig. S4A (ESI†), all the particles exhibited the flower-like structure, suggesting that the large-scale preparation of flower-like particles is possible. The mean diameter of each nodule was measured to be 355 ± 12 nm, and the number of PS nodules per seed was 8 on average. However, the use of the seeds with Q_{MPS} of 4.5 μmol m^{-2} formed the spherical particles with MPS-treated seed cores and PS shells (Fig. 2C). The mean diameter of the spheres was 752 ± 21 nm. For all the spheres, encapsulation of the seeds was observed, as shown in Fig. S4B.† This structural change can be explained using the difference in Q_{MPS} value. When Q_{MPS} is high, the increased affinity of PS to the functionalized seed surfaces allows the collapsing of growing polymer chains or the coalescence of freshly nucleated polymer domains, eventually forming a polymer shell fully coating the seeds.[34] For low Q_{MPS}, however, the high interfacial energy between the seed and PS blocks the spreading of the PS chains on the surfaces of the seeds or the merging of the polymer domains, consequently generating the polymer nodules around the seeds.[33]

The spherical particles in Fig. 2C were additionally treated at 70 °C for 2 h together with decane, EHMA, and AIBN for their transformation into bowl-like structure. At the elevated

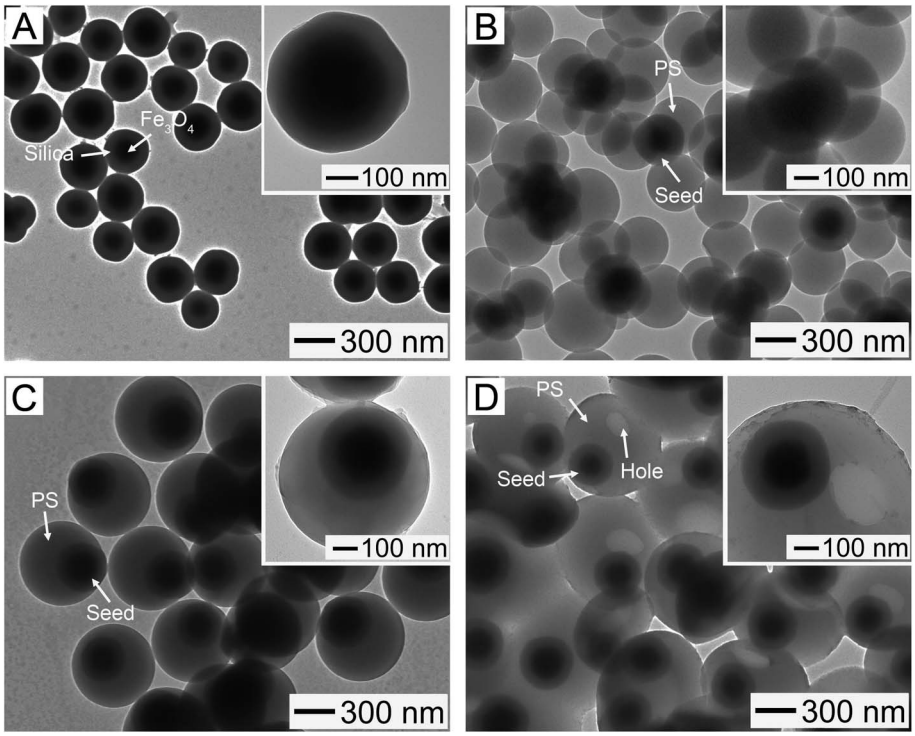

Fig. 2 (A) TEM image of the silica-coated Fe_3O_4 magnetic clusters obtained using the Stöber method. (B) TEM image of the flower-like particles obtained after the polymerization at 70 °C for 6 h in the presence of the MPS-treated seeds with Q_{MPS} of 1 μmol m^{-2}. (C) TEM image of the spherical particles made by the polymerization at 70 °C for 6 h in the presence of the MPS-treated seeds with Q_{MPS} of 4.5 μmol m^{-2}. (D) TEM image of the particles made by treating the spheres in (C) at 70 °C for 2 h, together with decane, EHMA, and AIBN.

temperature, the decane molecules tend to absorb into the polymer phase. Due to the phase separation between the absorbed molecules and polymer phase, the small-sized decane domains starts to form within the polymer, followed by merging into single-phased interiors over time. The interior voids and surface holes are created during the removal of decane.[19] Fig. S5 (ESI†) shows an SEM image of the particles obtained through the thermal treatment and washing in ethanol and isoamyl alcohol, demonstrating that the core–shell spheres were successfully transformed into bowl-like particles with hollow voids and large surface openings. The formation of the voids and open holes could be more clearly observed in the TEM image of Fig. 2D. Furthermore, it turned out that each seed with a magnetic cluster and a silica shell was still encapsulated in the bowl-like particle after the transformation, as shown in the inset TEM image, indicating that a sequence of treatments, such as MPS modification, polymerization, and transformation, did not affect the structure of the seed. Maintaining the seed structure rendered the polymer bowls magnetically responsive (Fig. S6, ESI†), with a saturation magnetization of 51.2 emu g^{-1} (Fig. S1†) that was much higher than the result reported in a previous study.[12] Similar results were observed in the flower-like and spherical particles, as shown in the insets in Fig. 2B and C, along with Fig. S6.†

To provide a catalytic property to the magnetic polymer particles, we immobilized AgNPs on the polymer particles owing to their low cost, unique reactivity and selectivity, and good stability, as well as recyclability in catalytic reactions.[35] Before the immobilization, Fe^{3+} and TA were consecutively deposited on the magnetic polymer particles. When Fe^{3+} was injected into the dispersion of the magnetic polymer particles, the cation was adsorbed on the negatively charged particles, which led to the change in their zeta potential (Fig. S7, ESI†). Subsequently, the addition of TA, which is a green reducing agent, induced the chelation of the molecules with the Fe^{3+} layer. The repetition of this process formed a highly stable coating of TA–Fe with good uniformity on the surfaces of the magnetic polymer particles, which could provide a homogeneous reduction environment on the highly curved surfaces.[36] When $Ag(NH_3)_2^+$ was injected into the dispersion of the magnetic polymer particles treated with Fe^{3+} and TA, the *in situ* reduction of the ion occurred on the magnetic polymer particles because of the catechol groups in TA molecules deposited on the particles.

Fig. 3A shows an SEM image of the resultant sample after the repeated deposition of Fe^{3+} and TA on the particles of Fig. S5,† followed by the reduction process. The particles exhibited the uniform distribution without aggregation and the bowl-like structure with hollow interior and large surface opening, which suggest no structural change after a series of processes involving the deposition and reduction. The TEM image in the inset shows the formation of the small spherical NPs on the surface of the magnetic polymer bowl. They exhibited a good uniformity in size, with a mean diameter of 6 nm. To investigate the elements present in the bowls, EDS analysis was carried out. C, O, Fe, Si, and Ag were observed (Fig. S8, ESI†). The existence of these elements was also confirmed using XPS measurement,

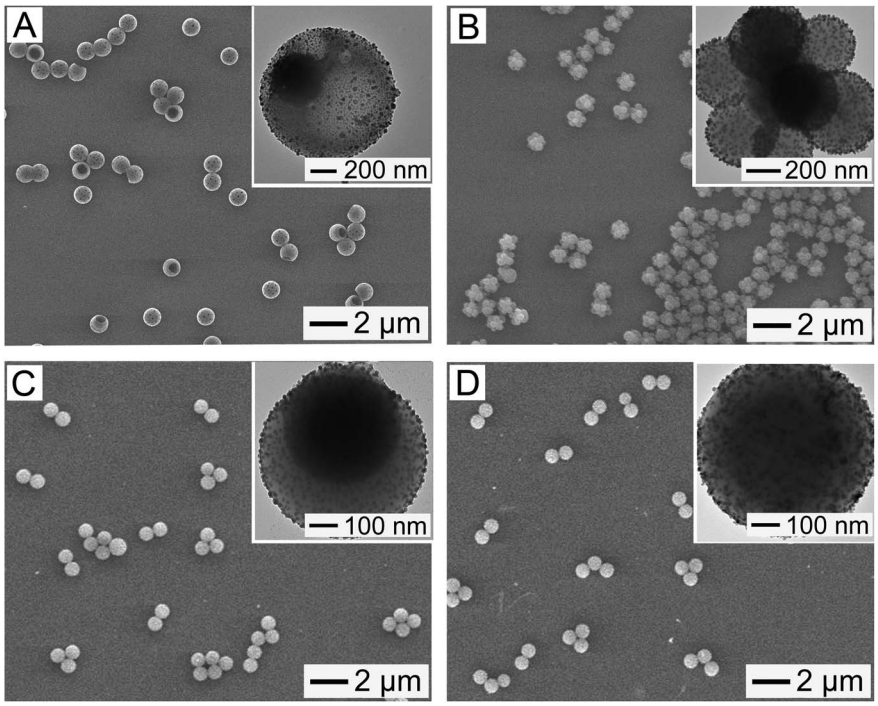

Fig. 3 SEM and TEM (inset) images of the polymer particles obtained after the repeated deposition of Fe^{3+} and TA, followed by the reduction of Ag precusor: (A) magnetic polymer bowls, (B) magnetic polymer flowers, (C) magnetic polymer spheres, and (D) polymer spheres without the magnetic cluster seeds.

as shown in Fig. S9 (ESI†), which suggests the *in situ* formation of AgNPs. These AgNP-immobilized, magnetic polymer bowl still retained a high magnetization (Fig. S1†), which suggests that their rapid recovery from reaction system is achievable using a magnet. Similar results were observed for the magnetic polymer flowers and spheres. They could immobilize AgNPs on their surfaces without any structural change, as shown in Fig. 3B and C. Furthermore, the AgNP-immobilized, non-magnetic polymer spheres were prepared using PS particles with a mean diameter of 750 ± 18 nm (Fig. 3D).

We examined the catalytic performance of these particles for the reduction of 4-NP. After the AgNP-immobilized, magnetic polymer spheres in Fig. 3C were introduced into an aqueous system containing 4-NP and $NaBH_4$, the temporal change of UV-vis absorbance spectra at 25 °C for the system was monitored (Fig. 4A). While the intensity located at 400 nm (I_{400}) decreased over time, a new peak started to appear at 300 nm and its intensity increased gradually, indicating that 4-AP formed as a resultant product from the reduction of 4-NP.[36] A similar reduction behavior was observed in the AgNP-attached polymer spheres (Fig. 4B). In contrast, there was no change in I_{400} in the absence of the AgNP-attached, magnetic polymer spheres (Fig. S10A, ESI†). The addition of the magnetic polymer spheres without immobilized AgNPs exhibited no change in I_{400}, either (Fig. S10B†). These results indicate that the reduction of 4-NP was induced by the attached AgNPs, which can assist the electron transfer from BH_4^- to the dye molecules adsorbed on the NPs.[12] Interestingly, the reduction behavior of 4-NP was more enhanced under the use of the magnetic polymer flowers and bowls with immobilized AgNPs (Fig. 4C and D). The I_{400} values for the flowers and bowls decreased by 67 and 85% in the initial 10 min, whereas the magnetic polymer spheres with immobilized AgNPs exhibited a decrease in I_{400} by 46% during the same period. Assuming that each magnetic polymer particle with immobilized AgNPs worked as each catalytic center, we could determine the turnover frequency (TOF), which quantifies the specific activity of a catalytic center for a reaction under defined conditions,[37] of the AgNP-immobilized magnetic polymer particles (see ESI†). The TOF value for the magnetic polymer bowl with attached AgNPs was calculated to be 3.01×10^{11} min^{-1}, which was larger than those for the other magnetic particles (9.11×10^{10} min^{-1} for the magnetic polymer sphere and 1.61×10^{11} min^{-1} for the magnetic polymer flower). This result indicates that the magnetic polymer bowl-based system had more enhanced catalytic activity for the reduction of 4NP than the other particles.

To further study the catalytic performance of the AgNP-attached particles in Fig. 3, we also examined the reduction behaviors at 25 °C of rhodmaine B and MB under the use of these particles. As shown in Fig. 5, all the samples exhibited a gradual decrease in I_{554} over time, indicating the reduction of rhodamine B.[6,12] However, the reduction rate differed in each sample. As in the case of the 4-NP, the fastest reduction was observed in the bowl sample, with a decrease in I_{554} by 74%, followed by the magnetic polymer flower (52% decrease) after the initial 10 min. Conversely, the magnetic and non-magnetic polymer spheres exhibited very slow reduction reactions, with I_{554} decrease by 34%. The catalytic reduction order was also same in the case of MB (Fig. 6).

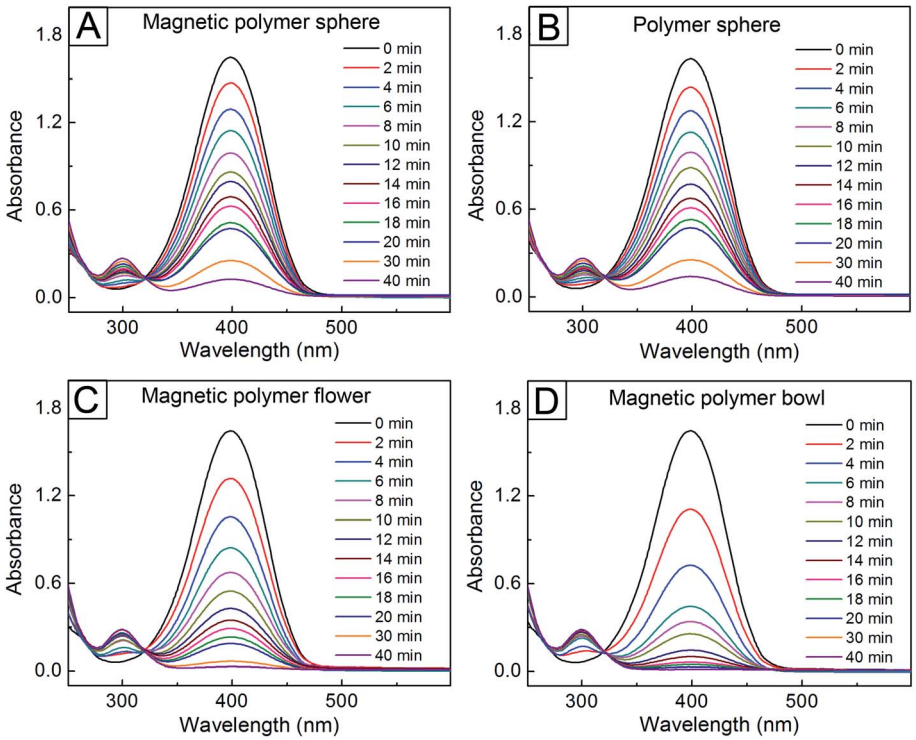

Fig. 4 Changes in UV-vis absorbance spectra at 25 °C over time of 4-NP using various particles with immobilized AgNPs: (A) magnetic polymer spheres, (B) polymer spheres without the magnetic cluster seeds, (C) magnetic polymer flowers, and (D) magnetic polymer bowls.

Additionally, the reduction of these organic dyes was examined at different temperatures (4 and 37 °C), as shown in Fig. S11–S16 (ESI†). In all the reduction tests, because the concentration of $NaBH_4$ was one hundred times higher than that of each dye, it could be assumed that the reduction of the dye molecules was not affected by the change in the

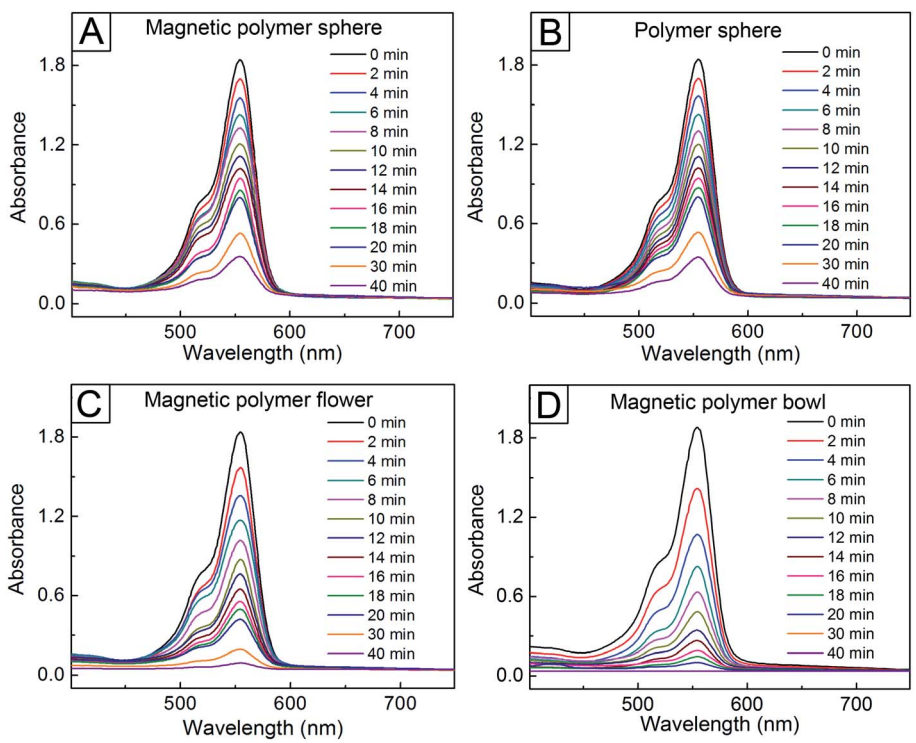

Fig. 5 Changes in UV-vis absorbance spectra at 25 °C over time of rhodamine B using various particles with immobilized AgNPs: (A) magnetic polymer spheres, (B) polymer spheres without the magnetic cluster seeds, (C) magnetic polymer flowers, and (D) magnetic polymer bowls.

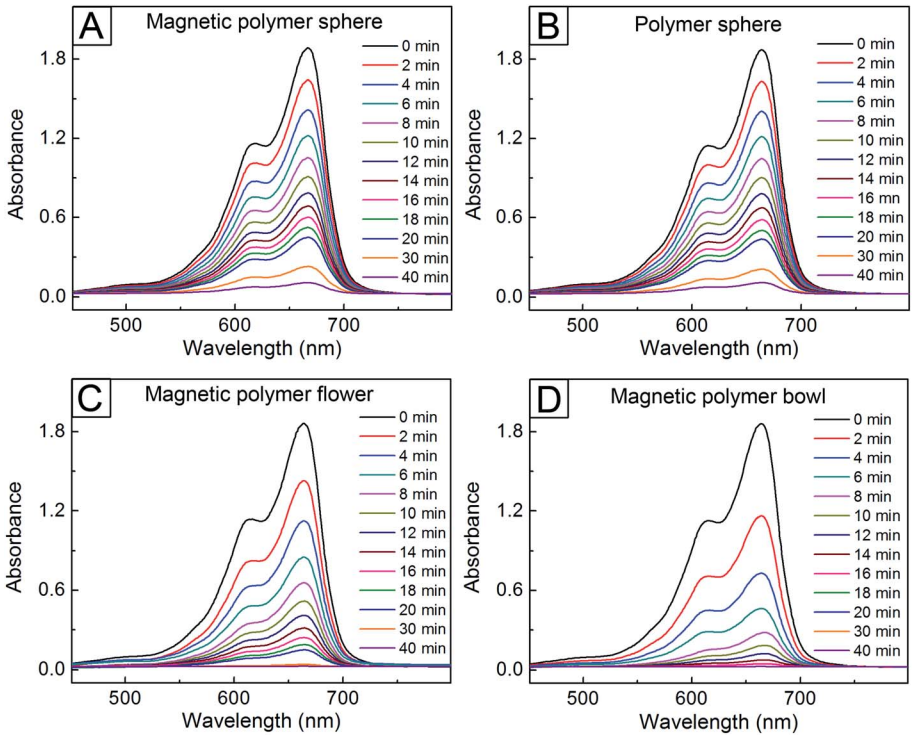

Fig. 6 UV-vis absorbance spectra at 25 °C for MB over time under the use of various particles with immobilized AgNPs: (A) magnetic polymer spheres, (B) polymer spheres without the magnetic cluster seeds, (C) magnetic polymer flowers, and (D) magnetic polymer bowls.

concentration of $NaBH_4$ during the whole reactions. Under this assumption, the first-order reaction kinetics could be used to understand the reduction of the dyes. Based on the linear relation between $-\ln(I_t/I_0)$, where I_t and I_0 are the absorbance peak intensities at time t and zero, and the time for each reaction (Fig. S17–S19, ESI†), the reaction rate constant (k) for each reduction system was evaluated. From the obtained value of k, the activation energy (E_a) for the reduction reaction of each dye could be estimated using the Arrhenius equation, *i.e.*, $\ln k = \ln A - E_a/RT$, where A and R denote the pre-exponential factor and ideal gas constant, respectively. For 4-NP, the k values at 4, 25, and 37 °C for the magnetic polymer bowls were 0.082, 0.202, and 0.319 min^{-1}, which were larger than those at the corresponding temperatures for the other particles (Table 1). Furthermore, the k value at 25 °C was higher than the results reported in previous studies.[38–41] The high k value for the magnetic polymer bowls was also observed in rhodamine B and MB. Conversely, the E_a values for the reduction of each dye were similar, irrespective of the type of AgNP-immobilized particles, which suggests that the reduction mechanism of each dye was the same for all the particle types. It is well known that the catalytic reduction of dye molecules, including 4-NP, rhodamine B, and MB, in the presence of $NaBH_4$ takes place on the surface of noble metal nanocatalysts.[42–44] BH_4^- ions, which are

Table 1 Reaction rate constant (k) at different temperatures and activation energy (E_a) for the reduction of various dyes driven by AgNP-immobilized particles with different structures

		k (min^{-1})			
Dye	Particle	4 °C	25 °C	37 °C	E_a (kJ mol^{-1})
4-NP	Non-magnetic sphere	0.025	0.062	0.098	29.6
	Magnetic sphere	0.024	0.061	0.101	30.2
	Magnetic flower	0.043	0.108	0.179	30.5
	Magnetic bowl	0.082	0.202	0.319	29.2
Rhodamine B	Non-magnetic sphere	0.014	0.042	0.073	35.8
	Magnetic sphere	0.014	0.042	0.073	35.8
	Magnetic flower	0.023	0.073	0.130	37.4
	Magnetic bowl	0.046	0.142	0.244	36.3
MB	Non-magnetic sphere	0.030	0.073	0.115	29.1
	Magnetic sphere	0.030	0.070	0.112	28.5
	Magnetic flower	0.051	0.127	0.199	29.0
	Magnetic bowl	0.096	0.231	0.366	28.9

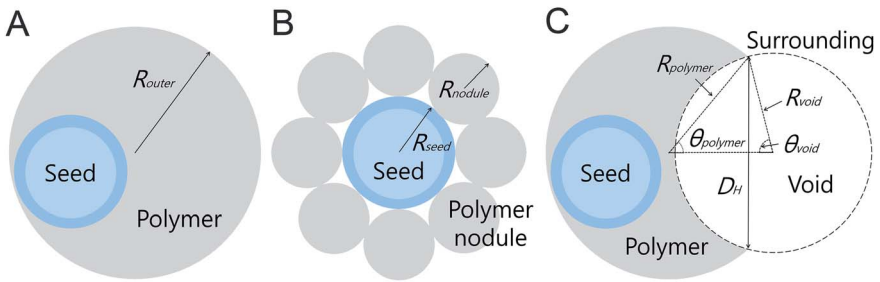

Scheme 2 Schematic illustration of magnetic polymer particles for calculating their volumes and surface areas: (A) sphere, (B) flower, and (C) bowl.

produced from ionization of $NaBH_4$, are adsorbed on the surface of the nanocatalysts, forming surface-bound hydrogen as metal hydride. At the same time, the dye molecules are also attached on the surface of the nanocatalysts. The hydrogen interacts with the adsorbed dye molecules, causing their reduction to 4-AP, leuco methylene blue, and leuco rhodamine B.[9,42,45] As shown in Table 1, the E_a values for all the organic dyes were in the range of 8–40 kJ mol^{-1}, corresponding to the result of surface catalyzed reactions,[46] which suggests that surface catalysis induced the reduction of the dye molecules.

To understand the higher k value in the magnetic polymer bowls for all the dyes, we calculated the volume (V) and surface area (S) of a magnetic polymer bowl, followed by comparing the values with those of the other-structured particles. For the calculation of V and S of each type of magnetic polymer particle, simple models were used, as illustrated in Scheme 2. For the magnetic polymer sphere, a simple model, consisting of the silica-coated Fe_3O_4 seed and surrounding polymer, was considered (Scheme 2A). The V and S of a magnetic polymer sphere can be expressed as $V = (4/3)\pi R_{outer}^3$ and $S = 4\pi R_{outer}^2$, where R_{outer} denotes the outer radius of the sphere, which could be determined using the TEM images of the magnetic polymer spheres. For the magnetic polymer flower, V can be expressed as $V = (4/3)\pi R_{seed}^3 + (4/3)\pi R_{nodule}^3 N_{nodule}$, where R_{seed}, R_{nodule}, and N_{nodule} denote the radius of the magnetic seed, radius of the polymer nodule, and number of polymer nodule attached to the magnetic seed, respectively (Scheme 2B). Assuming that the surface of the silica-coated magnetic core is fully covered with polymer nodules, the S of a magnetic flower can be expressed as $S = 4\pi R_{nodule}^2 N_{nodule}$. The V and S of the flower could be estimated from the R_{seed}, R_{nodule}, and N_{nodule} values obtained using the TEM images of the magnetic polymer flowers. In the case of the magnetic polymer bowl, V can be expressed as $V = (1/3)\pi R_{polymer}^3(2 + 3\cos\theta_{polymer} - \cos^3\theta_{polymer}) - (1/3)\pi R_{void}^3(2 - \cos\theta_{void} + \cos^3\theta_{void})$,[47] where $R_{polymer}$ and R_{void} denote the radii of the magnetic core-encapsulated polymer and void phases, respectively, and $\theta_{polymer}$ and θ_{void} are the angles opposite to the line segment connecting from the intersection of the two phases to center of each phase (Scheme 2C). Assuming that there is no loss of polymer chains during the transformation into bowl-like particles, its volume is the same as that of a magnetic polymer sphere. The S of a magnetic polymer bowl can be expressed as $S = 4\pi R_{polymer}^2 - 2\pi R_{polymer}^2(1 - \cos\theta_{polymer}) + 2\pi R_{void}^2(1 - \cos\theta_{void})$.[19] The additional relations among $R_{polymer}$, R_{void}, $\theta_{polymer}$, and θ_{void} are given as $D_H = 2R_{polymer}\sin\theta_{polymer} = 2R_{void}\sin\theta_{void}$ by taking the diameter of the single opening (D_H) on the surface of the bowl into consideration. The value of $\theta_{polymer}$ could be theoretically calculated using $R_{polymer}$ and D_H, which were determined from the TEM images for the magnetic polymer bowls. Taking the V of the magnetic polymer sphere together with D_H, the values of R_{void} and θ_{void} could be estimated. Using the obtained $\theta_{polymer}$, θ_{void}, $R_{polymer}$, and R_{void} values, we calculated S of the magnetic polymer bowl. Fig. S20 (ESI†) shows the calculated V for each type of magnetic polymer particle. The values of V for the non-magnetic polymer sphere and magnetic polymer particles (sphere, flower, and bowl) were very similar to each other, whereas the S values were different. As shown in Fig. 7A, the magnetic polymer bowl exhibited the largest S value (5.86×10^6 nm^2), followed by the magnetic flower and both the spheres.

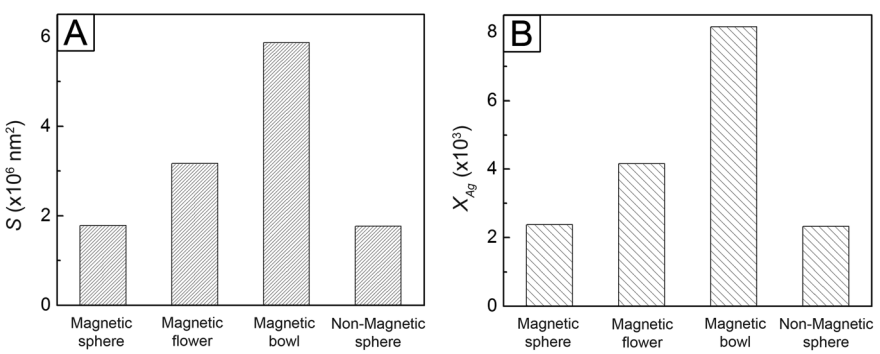

Fig. 7 (A) Surface areas (S) for the different types of magnetic polymer particles. (B) Numbers of immobilized AgNPs per magnetic polymer particle (X_{Ag}).

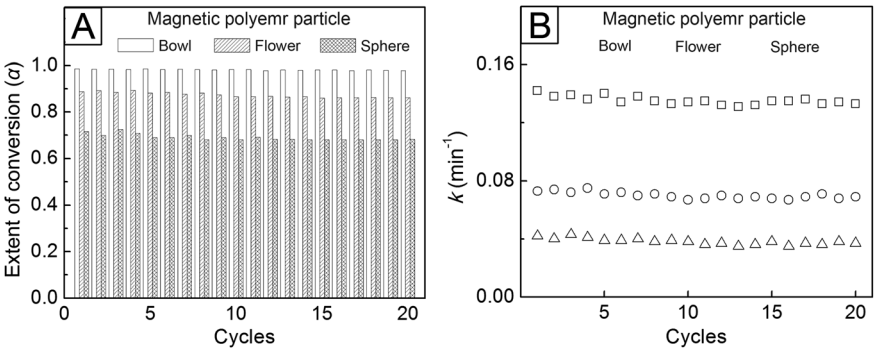

Fig. 8 (A) Conversion extent of rhodamine B (α) after its reduction for 30 min. (B) Reaction rate constants (k) during twenty reduction cycles of rhodamine B in the presence of the magnetic polymer particles.

Furthermore, we evaluated the number of AgNPs immobilized on one magnetic polymer particle (X_{Ag}) *via* ICP-MS analysis (see ESI†). The X_{Ag} for all the polymer particles with attached AgNPs is shown in Fig. 7B. The value of X_{Ag} of the magnetic polymer bowl was 8.2×10^3, which was larger than those of the other particles. This result indicates that the bowls were able to more effectively immobilize the AgNPs on their surfaces. To correlate the obtained S and X_{Ag} values, the normalization for S and X_{Ag} was conducted. As shown in Fig. S21 (ESI†), the normalized values in S for the magnetic polymer particles were consistent of those in X_{Ag} for the corresponding particles, which indicates that the openness of the bowls allowed the deposition of AgNPs on both their outer and inner surfaces. Moreover, the values were in good agreement with the normalized results in k, which were obtained by dividing k at each temperature for each type of magnetic polymer particles by that for the non-magnetic polymer spheres (Table 1). This similarity suggests that the larger surface area and openness of the magnetic polymer bowls led to the greater immobilization of AgNPs, which functioned as the reactive sites, thus inducing the enhanced catalytic activity and higher k value.

We also performed the reusability test of the magnetic polymer particles with immobilized AgNPs by examining their catalytic performances during repeated cycles of rhodamine B reduction. Upon the application of a magnet, the particles could be separated in 3 min from the reaction solution after each cycle of the reduction reaction and were then reused as catalysts. Fig. 8A shows the extent of conversion (α) of the organic dye, which is given as $\alpha = (I_0 - I_t)/I_0$, after the reaction for 30 min at 25 °C. The AgNP-attached, magnetic polymer bowls exhibited the highest α (over 0.98), and the values were similar for twenty cycles. Similarly, the high k value of the bowls was maintained even after the repeated reduction reactions (Fig. 8B). These results demonstrate the excellent stability and reusability of the magnetic polymer bowls with immobilized AgNPs, making them useful as a recoverable and efficient system for enhanced and repeated reduction of toxic organic dyes.

Conclusion

We have demonstrated the fabrication of AgNP-immobilized, magnetic polymer bowl for the enhancement of catalytic activity and recyclability. The use of silica-coated Fe_3O_4 magnetic clusters, which were prepared *via* modified solvothermal approach and the Stöber method, as seeds during seeded dispersion polymerization allowed the formation of magnetic polymer spheres and flowers. The additional phase-separation between the magnetic polymer spheres and decane led to their transformation into bowl-like particles still containing the magnetic clusters inside. Their larger surface area, compared with those of the magnetic spheres and flowers, and openness enabled a much higher immobilization of AgNPs on the surfaces. Such high immobilization endowed the bowls with an excellent catalytic activity for the reduction of 4-NP, rhodamine B, and MB. Moreover, the strong magnetic response, which was given by the magnetic clusters present in their inside, allowed a rapid, magnetic separation and an excellent reusability, achieving twenty cycled reduction of the dye molecules without loss of catalytic activity. Although this study mainly focused on the reduction of toxic organic dyes, these particles are applicable to the removal of pathogenic microorganisms owing to the bactericidal ability of highly immobilized AgNPs.[48] Moreover, the attachment of other functional nanoparticles can expand the applicability of the magnetic polymer bowls in diverse and advanced fields.

Conflicts of interest

The authors declare that they have no conflict of interest.

Acknowledgements

DCH thanks for the support from the National Research Foundation of Korea (NRF) grant funded by the Korea government (MSIT and MOE) (NRF-2018R1D1A1B07043878 and NRF-2021R1A2C1007129). GDM acknowledges the support from the Korea Institute of Industrial Technology through Development of fiber-based technology for reduction of hazardous substances in the air (kitech EO-21-0001).

References

1 F. Mushtaq, A. Asani, M. Hoop, X.-Z. Chen, D. Ahmed, B. J. Nelson and S. Pané, *Adv. Funct. Mater.*, 2016, **26**, 6995.

2 K. Naseem, Z. H. Farooqi, R. Begum and A. Irfan, *J. Cleaner Prod.*, 2018, **187**, 296.
3 K. G. Pavithra, P. S. Kumar, V. Jaikumar and P. S. Rajan, *J. Ind. Eng. Chem.*, 2019, **75**, 1.
4 S. Hamidouche, O. Bouras, F. Zermane, M. Houari, J. Debord, M. Harel, J.-C. Bollinger and M. Baudu, *Chem. Eng. J.*, 2015, **279**, 964.
5 Z. Wu, X. Yuan, H. Zhong, H. Wang, G. Zeng, X. Chen, H. Wang, L. Zhang and J. Shao, *Sci. Rep.*, 2016, **6**, 25638.
6 H. Veisi, S. B. Moradi, A. Saljooqi and P. Safarimehr, *Mater. Sci. Eng., C*, 2019, **100**, 445.
7 T. D. Raju, S. Veeralinggam and S. Badhulika, *ACS Appl. Nano Mater.*, 2020, **3**, 4777.
8 A. J. Kora and L. Rastogi, *Ind. Crops Prod.*, 2016, **1**, 1.
9 K. Naseem, R. Begum, W. Wu, A. Irfan, A. G. Al-Sehemi and Z. H. Farooqi, *J. Cleaner Prod.*, 2019, **211**, 855.
10 K. B. Narayanan and N. Sakthivel, *J. Hazard. Mater.*, 2011, **189**, 519.
11 Y. Liu, Y. Y. Zhang, Q. W. Kou, Y. Chen, D. L. Han, D. D. Wang, Z. Y. Lu, L. Chen, J. H. Yang and S. Xing, *RSC Adv.*, 2018, **8**, 2209.
12 Y. Wang, P. Gao, Y. Wei, Y. Jin, S. Sun, Z. Wang and Y. Jiang, *J. Environ. Manage.*, 2021, **278**, 111473.
13 M. Gangarapu, S. Sarangapany, K. K. Veerabhali, S. P. Devipriya and V. B. R. Arava, *J. Cluster Sci.*, 2017, **28**, 3127.
14 C. Jin, Y. Qu, M. Wang, J. Han, Y. Hu and R. Guo, *Langmuir*, 2016, **32**, 4595.
15 Y. Lee, M. A. Garcia, N. A. F. Huls and S. Sun, *Angew. Chem., Int. Ed.*, 2010, **49**, 1271.
16 Y. Chi, Q. Yuan, Y. Li, J. Tu, L. Zhao, N. Li and X. Li, *J. Colloid Interface Sci.*, 2012, **383**, 96.
17 M. Oćwieja, D. Lupa and Z. Adamczyk, *Langmuir*, 2018, **34**, 8489.
18 Y. Li, Y. Hu, S. Ye, Y. Wu, C. Yang and L. Wang, *New J. Chem.*, 2016, **40**, 10398.
19 D. I. Kim, J. H. Park, H. Seo, S. G. Hong, H. J. Kim, H. Ahn, J. Kim, G. D. Moon and D. C. Hyun, *J. Ind. Eng. Chem.*, 2020, **82**, 439.
20 Z. Deng, H. Zhu, B. Peng, H. Chen, Y. Sun, X. Gang, P. Jin and J. Wang, *ACS Appl. Mater. Interfaces*, 2012, **4**, 5625.
21 M. Schrinner, S. Proch, Y. Mei, R. Kempe, N. Miyajima and M. Ballauff, *Adv. Mater.*, 2008, **20**, 1928.
22 Y. Li, Y. Wu, Y. Gao, S. Sha, J. Hao, G. Cao and C. Yang, *RSC Adv.*, 2013, **3**, 26361.
23 N. Zhang, X. Yu, J. Hu, F. Xue and E. Ding, *RSC Adv.*, 2013, **3**, 13740.
24 T. Xu, Y. Li, J. Zhang, Y. Qi, X. Zhao and Q. Zhang, *Appl. Surf. Sci.*, 2015, **345**, 264.
25 X. Ni, Z. Wu, X. Gu, D. Wang, C. Yang, P. Sun and Y. Li, *Langmuir*, 2017, **33**, 8157.
26 Y. Zhao, J. Feng, L. Hong, Y. Li, C. Wang and S. Ye, *Inorg. Chem. Front.*, 2018, **5**, 1133.
27 R. A. Ramli, *RSC Adv.*, 2017, **7**, 52632.
28 J. Gao, X. Ran, C. Shi, H. Cheng, T. Cheng and Y. Su, *Nanoscale*, 2013, **5**, 7026.
29 J. Ge, Y. Hu, M. Biasini, W. P. Beyermann and Y. Yin, *Angew. Chem., Int. Ed.*, 2007, **46**, 4342.
30 M. F. Casula, Y.-W. Jun, D. J. Zaziski, E. M. Chan, A. Corrias and A. P. Alivisatos, *J. Am. Chem. Soc.*, 2006, **128**, 1675.
31 H. Deng, X. Li, Q. Peng, X. Wang, J. Chen and Y. Li, *Angew. Chem., Int. Ed.*, 2005, **117**, 2842.
32 W. Stöber, A. Fink and E. Bohn, *J. Colloid Interface Sci.*, 1968, **26**, 62.
33 E. Bourgeat-Lami, M. Insulaire, S. Reculusa, A. Perro, S. Ravaine and E. Duguet, *J. Nanosci. Nanotechnol.*, 2006, **6**, 432.
34 Y. Li and B. Liu, *ACS Macro Lett.*, 2017, **6**, 1315.
35 X. Du, J. He, J. Zhu, L. Sun and S. An, *Appl. Surf. Sci.*, 2012, **258**, 2717.
36 D. Li, X. Xu, X. Wang, R. Li, C. Cai, T. Sun, Y. Zhao, L. Chen, J. Xu and N. Zhao, *ACS Appl. Nano Mater.*, 2019, **2**, 3510.
37 H. Jia, X. Gao, Z. Chen, G. Liu, X. Zhang, H. Yan, H. Zhou and L. Zheng, *CrystEngComm*, 2012, **14**, 7600.
38 R. Das, V. S. Sypu, H. K. Paumo, M. Bhaumik, V. Maharaj and A. Maity, *Appl. Catal., B*, 2019, **244**, 546.
39 S. Zhang, S. Gai, F. He, Y. Dai, P. Gao, L. Li, Y. Chen and P. Yang, *Nanoscale*, 2014, **6**, 7025.
40 A. Mondal, A. Mondal, B. Adhikary and D. K. Mukherjee, *Bull. Mater. Sci.*, 2017, **40**, 321.
41 J. G. You, C. Shanmugam, Y. W. Liu, C. J. Yu and W. L. Tseng, *J. Hazard. Mater.*, 2017, **324**, 420.
42 J. Piella, F. Merkoçi, A. Genç, J. Arbiol, N. G. Bastus and V. Puntes, *J. Mater. Chem. A*, 2017, **5**, 11917.
43 K. Zhang, J. M. Suh, J.-W. Choi, H. W. Jang, M. Shokouhimehr and R. S. Varma, *ACS Omega*, 2019, **4**, 483.
44 R. Grzeschik, D. Schafer, T. Holtum, S. Küpper, A. Hoffmann and S. Schlücker, *J. Phys. Chem. C*, 2020, **124**, 2939.
45 T. Jeyapragasam and R. S. Kannan, *Russ. J. Phys. Chem. A*, 2016, **90**, 1334.
46 S. K. Das, M. M. R. Khan, A. K. Guha and N. Naskar, *Green Chem.*, 2013, **15**, 2548.
47 J. H. Son, D. I. Kim, J. H. Park, H. Seo, S. G. Hong, J. H. Choi, J. Kim, G. D. Moon and D. C. Hyun, *Polymer*, 2019, **167**, 85.
48 J. Parmar, D. Vilela, K. Villa, J. Wang and S. Sánchez, *J. Am. Chem. Soc.*, 2018, **140**, 9317.